coatings

MDPI

Article

Manipulation of Magnetization Reversal by Electric Field in a FePt/(011)PMN-PT/Au

Xiaoyu Zhao [1,2], Yaxin Yan [1,3], Jiahong Wen [3], Xiaolong Zhang [4] and Dunhui Wang [2,3,*]

1 Key Laboratory of Novel Materials for Sensor of Zhejiang Province, Institute of Advanced Magnetic Materials, College of Materials & Environmental Engineering, Hangzhou Dianzi University, Hangzhou 310018, China; zhaoxy@hdu.edu.cn (X.Z.); yanyaxin2021@163.com (Y.Y.)
2 National Laboratory of Solid State Microstructures, Nanjing University, Nanjing 210093, China
3 The College of Electronics and Information, Hangzhou Dianzi University, Hangzhou 310018, China; wenjiahong@hdu.edu.cn
4 Key Laboratory of Functional Materials Physics and Chemistry, Ministry of Education, College of Physics, Jilin Normal University, Changchun 130103, China; zhangxiaolong@jlnu.edu.cn
* Correspondence: wangdh@nju.edu.cn

Abstract: Electric field manipulation of magnetism and 180° magnetization reversal are crucial for realizing magnetic storage devices with low-power consumption. Here, we demonstrate that electric-field manipulation of magnetic anisotropy rotation is achieved by the strain-mediated magnetoelectric effect in a $Fe_{50}Pt_{50}$/(011)0.7Pb($Mg_{1/3}Nb_{2/3}$)O_3–0.3$PbTiO_3$/Au. The remanent magnetization and magnetic coercivity of the $Fe_{50}Pt_{50}$ film exhibit an obvious response with the change of the electric fields. Moreover, the reversible in-plane 180° magnetization reversal can be controlled by alternating on or off the electric field under a small bias magnetic field. These results suggest a promising application for realizing magnetoelectric random access memory (MeRAM) devices with low-power consumption.

Keywords: magnetoelectric effect; PMN-PT; electric field manipulation of magnetism; magnetic anisotropy rotation; reversible 180° magnetization reversal

check for updates

Citation: Zhao, X.; Yan, Y.; Wen, J.; Zhang, X.; Wang, D. Manipulation of Magnetization Reversal by Electric Field in a FePt/(011)PMN-PT/Au. *Coatings* **2021**, *11*, 730. https://doi.org/10.3390/coatings11060730

Academic Editor: Alessio Lamperti

Received: 4 May 2021
Accepted: 4 June 2021
Published: 17 June 2021

1. Introduction

With the rapid development of electronic information, the demand for information memory devices with high speed, high density, and low power consumption is increasingly urgent. At present, many kinds of memory devices are widely concerned, such as magnetoresistive random access memory (MRAM) [1], resistance random access memory (RRAM) [2–5], ferroelectric random access memory (FRAM) [6], based on the spin-orbit torque MRAM or spin-transfer torque MRAM [1,7–9], etc. The control of magnetism is a fundamental process for current MRAM devices, which encode two different magnetic states for the recording media corresponding to "0" and "1", respectively [10,11]. The two magnetic states can be tuned and reversed by magnetic fields, which require coils with electric current, making the system bulky and consuming a lot of energy [10,12]. Thus, it is a pressing need to modulate and switch magnetization by nonmagnetic means. Compared to the magnetic field tunable devices, electric field control of devices are much more compact, lightweight, and energy efficient [12,13]. Therefore, the electric-field control of magnetism is extensively investigated and has great potential in magnetoelectric random access memory (MeRAM), which combines the advantages of MRAM and FRAM [14]. In the magnetoelectric (ME) heterostructures with a ferromagnetic (FM) thin film growing on a ferroelectric (FE) substrate (for example, metal/[Pb($Mg_{1/3}Nb_{2/3}$)O_3](1–x)–[$PbTiO_3$]x), the strain-mediated converse ME effect acts as a main mechanism [15–20], i.e., using the electric-field-induced strain from the FE layer, the magnetism of the FM thin film can be controlled by modifying magnetic anisotropy [21–27], altering the exchange coupling [28–30] or driving magnetic phase transition [31–33]. Thus, using an electric field instead of a traditional magnetic field is feasible to manipulate the magnetism in the design of low-power consumption MeRAM devices [21,23,24,34–40].

Large magnetic response and reversible 180° magnetization reversal driven by the electric fields ensure the stability and signal-to-noise ratio of the magnetic signals, which have great significance for realizing MeRAM [21,24,29]. Many experiments and theoretical predictions have demonstrated that the 180° magnetization reversal can be realized by electric-fields-manipulated magnetic anisotropy rotation in a number of ME heterostructures [26,29,30,41–43]. For example, in the CoPt or FePd/(001)$Pb(Mg_{1/3}Nb_{2/3})O_3$–$PbTiO_3$ heterostructure, the magnetization vector reversal of the film can be switched by the variation of magnetic coercivity (H_c), which is caused by turning on or off the electric field [39,40]. However, large saturated magnetic fields are necessary for achieving the reversible 180° magnetization reversal in the aforementioned reports, which leads to high energy consumption. Therefore, realizing electric fields manipulating 180° magnetization reversal in a small bias magnetic field is greatly desirable.

In this paper, a $Fe_{50}Pt_{50}$ (FePt) film is chosen as the FM layer due to its large magnetic anisotropy [36]. A relaxor ferroelectrics (011) oriented $0.7Pb(Mg_{1/3}Nb_{2/3})O_3$–$0.3PbTiO_3$ (PMN-PT) single crystal is selected as the FE substrate, which has a large in-plane anisotropic piezoelectric response [44–46]. We demonstrate that electric-field control of magnetic anisotropy rotation, accompanied by a large ME effect, can be obtained in this FePt/(011)PMN-PT/Au. The remanent magnetization (M_r) and H_c of the FePt film along the [100] or [01−1] direction exhibit an obvious anisotropic response with the applying electric fields. Taking advantage of these properties, the 180° magnetization reversal can be controlled reversibly in this ME composite by alternating on or off the electric field around a bias magnetic field of 150 Oe. More importantly, this bias magnetic field is obviously smaller than the saturation magnetic field (750 Oe), which is meaningful for the design of low-power consumption MeRAM devices.

2. Experimental Section

A (011)-oriented PMN-PT single crystal substrate, which was prepared with the Bridgman method was commercially provided by Hefei Kejing Material Technology Co., Ltd. (Hefei, An Hui, China). The Fe (99.99%) and Pt (99.99%) targets were co-deposited on the commercial 10 mm × 5 mm × 0.5 mm (011)-oriented PMN-PT substrate to obtain the FePt film by using a magnetron sputtering system (JZCK-400DJ, Shenyang, Liao Ning, China). The distance between the Fe, Pt targets and the PMN-PT substrate was 10 cm. The base vacuum of the magnetron sputtering chamber was below 10^{-4} Pa. During the FePt film deposition, the PMN-PT substrate temperature was kept at 450 °C and the working Ar pressure was 0.6 Pa. The deposited power of Fe target and Pt target was 20 and 30 W, respectively. The composition of the co-deposited FePt film was $Fe_{50}Pt_{50}$, which was confirmed by scanning electron microscopy (SEM, JEOL 6500, Tokyo, Japan) equipped with energy dispersive spectroscopy (EDS). The FePt film with a thickness of 20 nm was determined by the stylus profiler (Veeco Dektak 150, New York, NY, USA). The 150 nm Au film was grown on the backside of the FePt/(011)PMN-PT as an electrode, which constructed the FePt/PMN-PT/Au. The surface morphology of FePt film was measured with scanning probe microscopy (SPM, Veeco, Dimension V, New York, NY, USA). A voltage source meter (Keithley, model 2410, Beaverton, OG, USA) was used to provide the electric fields applied between the FePt film and Au electrode. The strain properties of the FePt/PMN-PT/Au along in-plane [100] and [01−1] directions were recorded by the resistance strain gauge technique, respectively. The polarization hysteresis loop of the FePt/PMN-PT/Au was measured by a standard ferroelectric test unit (TF-2000, aix-ACCT, Aachen, Nordrhein-Westfalen, Germany). The magnetic properties of the FePt/PMN-PT/Au were characterized by a vibrating sample magnetometer (VSM, Microsense EV7, Lowell, MA, USA). The detailed measurement conditions for the FePt/PMN-PT/Au were reported in our earlier work [36].

3. Results and Discussion

Figure 1a shows the schematic diagram of strain measurement for the FePt/PMN-PT/Au. The strain gauges are adhered to the surface of FePt film along the in-plane [100] and [01−1] directions, respectively. The electric fields are applied along the [011] direction of the FePt/PMN-PT/Au. The electric field dependence of strain (S–E) curves along the in-plane two directions are shown in Figure 1b. With a symmetric electric-field sweeping from −10 to 10 kV/cm, the in-plane S-E curves exhibit symmetrical butterfly shaped behavior along the in-plane [100] and [01−1] directions, respectively. Meanwhile, the in-plane S–E curves of the FePt/PMN-PT/Au show highly anisotropic behavior due to its large anisotropic piezoelectric coefficients [21], leading to a compressive strain along the in-plane [100] direction and a tensile strain along the in-plane [01−1] direction [25,45,46]. The polarization hysteresis loop of the FePt/PMN-PT/Au is shown in Figure 1c, which exhibits ferroelectric performance with the remnant polarization of 32 μC/cm^2 and coercive field of 2 kV/cm. Figure 1d exhibits the surface morphology of FePt film deposited on the PMN-PT substrate, in which a smooth surface is observed. The aforementioned features provide a favorable condition for the following ME coupling measurements.

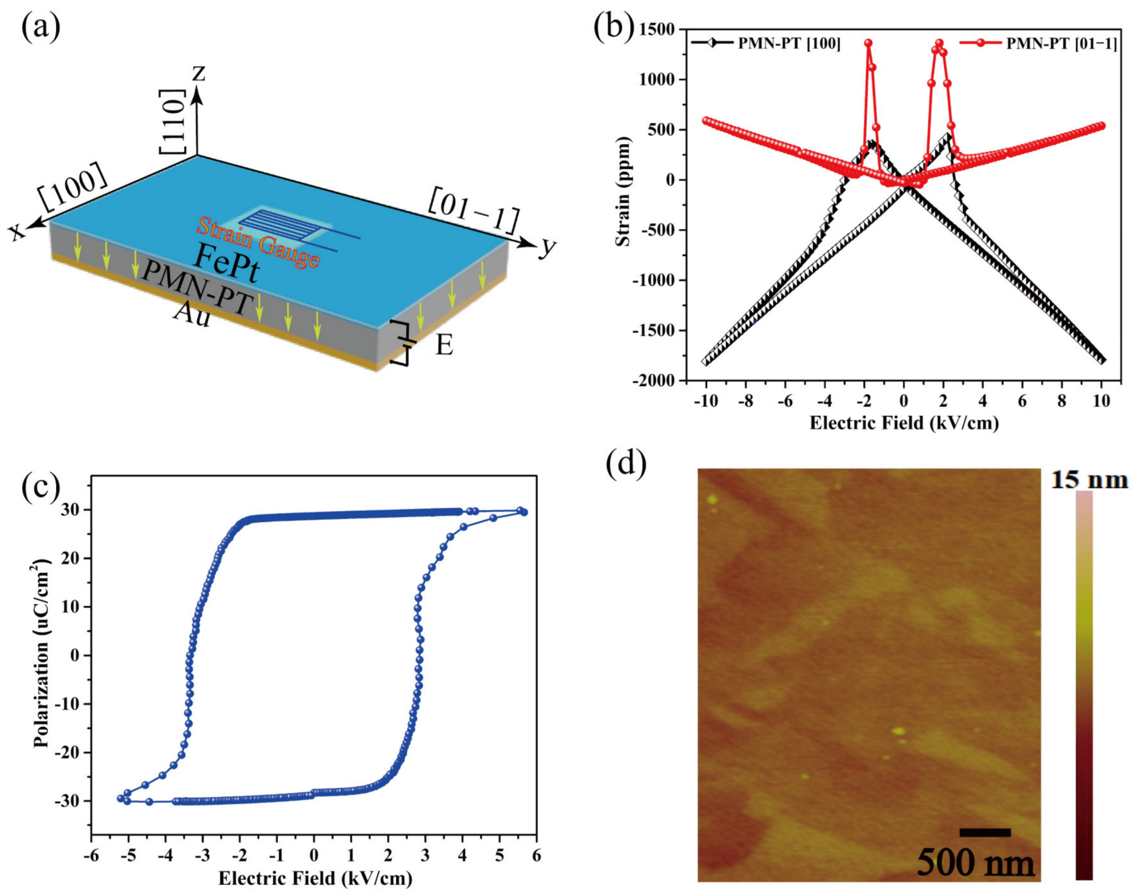

Figure 1. (**a**) Schematic diagram of strain measurement for the FePt/PMN-PT/Au under applied electric fields; (**b**) the electric field dependence of in-plane strain curves along the [100] and [01−1] directions, respectively; (**c**) the polarization hysteresis loop of the FePt/PMN-PT/Au at room temperature; (**d**) the surface morphology image of the FePt film with an area of 2 × 2 um^2.

Schematic images for magnetic hysteresis (M–H) loops measured under electric fields along both the in-plane [100] and [01−1] directions are shown in Figure 2a,b, respectively. The M–H loops of the FePt/PMN-PT/Au are characterized along the [100] and [01−1] directions with in situ electric fields of 0 kV/cm, 2 kV/cm, 4 kV/cm, 8 kV/cm, and 10 kV/cm, respectively. With the increase in the electric field, the magnetization process of the FePt film along the in-plane [100] direction becomes harder and displays a reduction in squareness ratio (M/M_s), which is shown in Figure 2c. However, the magnetic change along the in-plane [01−1] direction is just the converse, which has an increment of the squareness ratio under the same electric fields as shown in Figure 2d. An obvious electric-fields-driven in-plane magnetic anisotropy rotation behavior is observed, leading to the reorientation of the magnetic easy axis from the in-plane [100] direction to [01−1] direction. For further characterizing the ME effect in the FePt/PMN-PT/Au, the variation of M_r and H_c of the FePt film as a function of applying electric fields along both the in-plane [100] and [01−1] directions are shown in Figure 2e,f, respectively. When the electric field is 0 kV/cm, the magnetic easy axis is initially along the in-plane [100] direction, which reveals high M/Ms along the in-plane [100] direction and low M/Ms along the in-plane [01−1] direction. As shown in Figure 2e, the Mr changes remarkably with the electric field increasing to 10 kV/cm. The magnetization changing rate defined as $(M(E) - M(0))/M(0) \times 100\%$ is about +190% and –41% for the magnetic field applied along the in-plane [100] and [01−1] directions, respectively. Meanwhile, the H_c also shows an obviously response with the increase of electric field, which is shown in Figure 2f. Similarly, the change rate of H_c $(H_c(E) - H_c(0))/H_c(0) \times 100\%$ is about +137% along [01−1] direction, while the change rate along [100] direction is about –52% under the 10 kV/cm. This giant anisotropic rotation ability can be understood as the ultra-high in-plane anisotropic strain mediated ME effect, which leads to a rotation of the magnetic easy axis from the in-plane [100] direction to [01−1] direction [10,27]. Thus, the magnetization of FePt film along the two in-plane directions can be effectively manipulated by the electric-field-induced strains (compressive and tensile stress) so that M_r and H_c show an opposite behavior along in-plane [100] direction and [01−1] direction, respectively. The M_r and H_c with obvious changes along the two in-plane directions provide a potential opportunity to obtain reversible 180° magnetization reversal.

According to the earlier reports, the electric-field-induced magnetization reversal can be realized in the FePt film with the change of electric fields due to the variation of H_c [39,40]. We take the magnetization curve along [01−1] direction as an example to demonstrate this reversal process. First, the FePt/PMN-PT/Au is magnetized by a saturation magnetic field (750 Oe) along the [01−1] direction with an electric field applied on the substrate. Then, the magnetic field gradually reduces and goes through zero to a negative field $H_c(X)$ = 150 Oe, which locates between $H_c(0)$ and $H_c(E)$. If the applied electric field is removed at this time, the magnetization of FePt film would correspondingly drop from point A to point B and accompany with the change in sign of magnetization from +M to −M due to the different magnetization states under the electric fields of 10 kV/cm and 0 kV/cm [38–40]. It is worth noting that the magnetization vector is not fully reversed at this condition, which results in a relatively small signal-to-noise ratio. Now, if the magnetic field is switched off to 0 Oe, the sign of magnetization vector cannot be changed. In order to realize the reversible magnetization reversal, based on the earlier reports [39,40], the FePt film should be magnetized under a reverse saturation magnetic field, which corresponds to the movement from B to F. The switching back of magnetization from C to D can be achieved by analogous method, which is shown in detail in Figure 3a. Based on this mechanism, a relatively large saturation magnetic field is required to realize the reversible magnetization reversal [38–40].

In the following, we demonstrate that the 180° magnetization reversal can be achieved in this ME composite with a small bias magnetic field by alternating on or off the electric field. As shown in Figure 3b, after the magnetization vector changes from A to B by switching off the electric field, the magnetization vector can further drop to point H by switching on the electric field again, which just follows the magnetization curve under the electric field (green magnetization curve in Figure 3b). Keeping on the applying of this electric field, the magnetization vector would switch to point C as the magnetic field reverses from −150 Oe to 150 Oe. Based on the magnetization curves without and with the electric field, the magnetization vector would jump to point D and G by switching off and on the electric fields, respectively. It is worth pointing out that, from point H to point G, a 180° magnetization reversal is obtained in this FePt/PMN-PT/Au by alternating on or off the electric field. More importantly, unlike the earlier reports, the realization of this reversal process does not require the saturation magnetic field, which is shown in the loop of A–B–H–C–D–G. In the current operation, a relatively small bias magnetic field of 150 Oe instead of a saturation magnetic field of 750 Oe is used, which remarkably decreases energy consumption.

Figure 4 shows the repeatability of 180° magnetization reversal in the FePt/PMN-PT/Au. Under a small bias magnetic field of 150 Oe, by alternating on or off the electric field, the magnetization vector can switch from the positive to negative states again and again (loop of A–B–H–C–D–G), indicating good stability and repeatability, which is meaningful for realizing the MeRAM devices with lower power consumption.

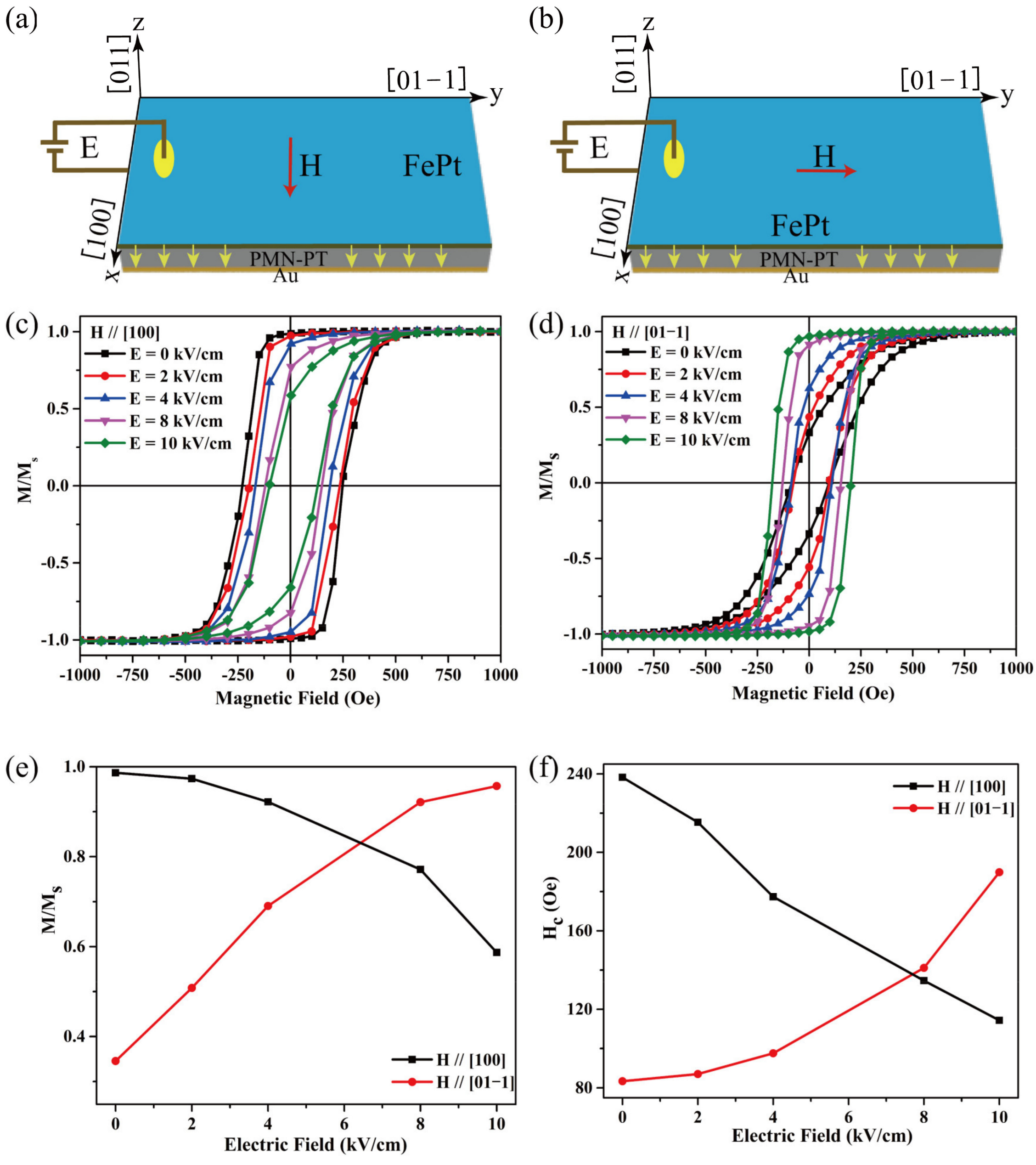

Figure 2. Schematic images for M–H loops measured under electric fields along the [100] direction (**a**) and [01−1] directions (**b**), respectively; the M–H loops measured under different electric fields along the [100] (**c**) and [01−1] (**d**) directions, respectively; electric-field controlled Mr and Hc along the [100] (**e**) and [01−1] (**f**) directions, respectively.

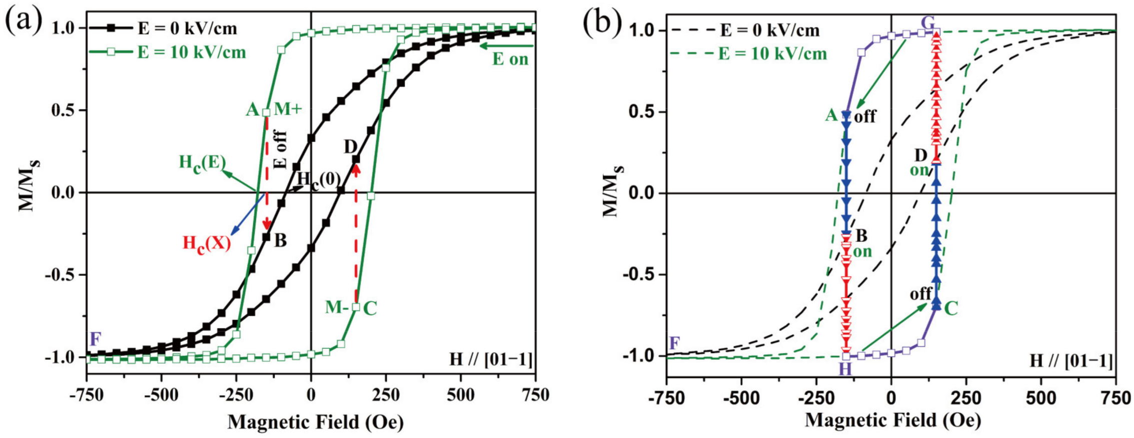

Figure 3. (**a**) The process of electric-field-manipulated magnetization vector switching by manipulating two magnetization states in the FePt/PMN-PT/Au; (**b**) the 180° magnetization reversal with a small bias magnetic field by alternating on or off electric field.

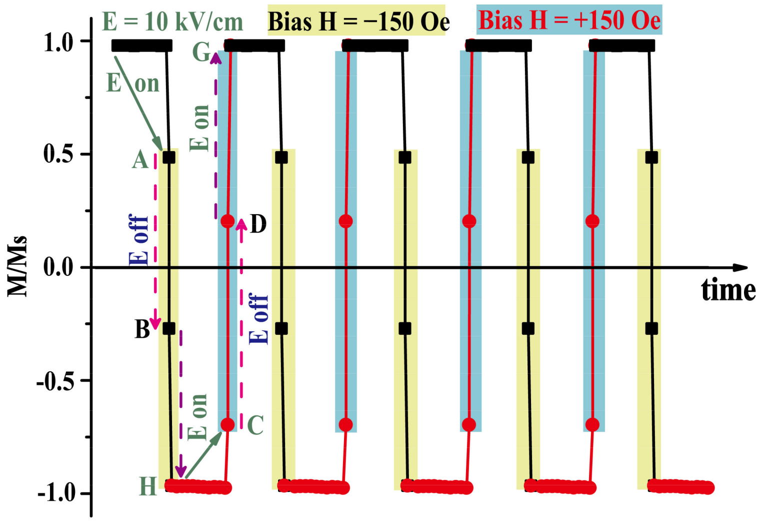

Figure 4. The repeatable 180° magnetization reversal response to alternating on and off electric fields under a small bias magnetic fields along the [01−1] direction.

4. Conclusions

We demonstrate that electric-field-control of magnetic anisotropy rotation can be achieved by the strain-mediated ME effect in a FePt/(011)PMN-PT/Au. The M_r and H_c of the FePt film along in-plane [100] and [01−1] directions exhibit an obvious anisotropic response with the increase in the electric field. Furthermore, taking advantage of the magnetic changes caused by the electric field, the reversible 180° magnetization reversal can be controlled by alternating on and off the electric fields under a small bias magnetic field of 150 Oe, which is obviously smaller than the saturation magnetic field (750 Oe). This 180° magnetization reversal recording process in the FePt/PMN-PT/Au is a promising approach for developing strain-mediated MeRAM devices with lower power consumption.

Author Contributions: Writing—original draft preparation, review and editing, X.Z. (Xiaoyu Zhao) and D.W.; methodology and data curation X.Z. (Xiaoyu Zhao) and Y.Y.; funding acquisition, J.W. and X.Z. (Xiaolong Zhang). All authors have read and agreed to the published version of the manuscript.

Funding: This work is supported by the National Natural Science Foundation of China (No. 51901060, 12004090); the National Natural Science Foundation of Zhejiang Province (No. LY21E010004, LQ21A040009); the Fundamental Research Funds for the Provincial Universities of Zhejiang (No.

GK209907299001-025), and the Ten Thousand Talents Plan of Zhejiang Province of China (Grant No. 2019R52014).

Institutional Review Board Statement: Not Applicable.

Informed Consent Statement: Not Applicable.

Data Availability Statement: The data provided in this study could be released upon logical requests.

Conflicts of Interest: The authors declare no conflict of interest.

References

1. Ikegawa, S.; Mancoff, F.B.; Janesky, J.; Aggarwal, S. Magnetoresistive Random Access Memory: Present and Future. *IEEE Trans. Electron Devices* **2020**, *67*, 1407–1419. [CrossRef]
2. Wong, H.S.P.; Lee, H.Y.; Yu, S.M.; Chen, Y.S.; Wu, Y.; Chen, P.S.; Lee, B.; Chen, F.T.; Tsai, M.J. Metal-Oxide RRAM. *Proc. IEEE* **2012**, *100*, 1951–1970. [CrossRef]
3. Gao, Z.M.; Huang, X.S.; Li, P.; Wang, L.F.; Wei, L.; Zhang, W.F.; Guo, H.Z. Reversible Resistance Switching of 2D Electron Gas at $LaAlO_3$/$SrTiO_3$ Heterointerface. *Adv. Mater. Interfaces* **2018**, *5*, 1701565. [CrossRef]
4. Tian, J.J.; Wu, H.J.; Fan, Z.; Zhang, Y.; Pennycook, S.J.; Zheng, D.F.; Tan, Z.W.; Guo, H.Z.; Yu, P.; Lu, X.B.; et al. Nanoscale Topotactic Phase Transformation in $SrFeO_x$ Epitaxial Thin Films for High-Density Resistive Switching Memory. *Adv. Mater.* **2019**, *31*, 1903679. [CrossRef] [PubMed]
5. Chen, Y.Y. ReRAM: History, Status, and Future. *IEEE Trans. Electron Devices* **2020**, *67*, 1420–1433. [CrossRef]
6. Scott, J.F.; Paz de Araujo, C.A. Ferroelectric Memories. *Science* **1989**, *246*, 1400–1405. [CrossRef] [PubMed]
7. Sun, Q.L.; Kwon, S.; Stamenova, M.; Sanvito, S.; Kioussis, N. Electric Field Modulation of Magnetism in Ferrimagnetic Heusler Heterostructures. *Phys. Rev. B* **2020**, *101*, 134419. [CrossRef]
8. Liu, L.; Qin, Q.; Lin, W.N.; Li, C.J.; Xie, Q.D.; He, S.K.; Shu, X.Y.; Zhou, C.H.; Lim, Z.S.; Yu, J.H.; et al. Current-induced Magnetization Switching in All-oxide Heterostructures. *Nat. Nanotechnol.* **2019**, *14*, 939–944. [CrossRef] [PubMed]
9. Tang, M.; Shen, K.; Xu, S.J.; Yang, H.L.; Hu, S.; Lü, W.M.; Li, C.J.; Li, M.S.; Yuan, Z.; Pennycook, S.J.; et al. Bulk Spin Torque-Driven Perpendicular Magnetization Switching in $L1_0$ FePt Single Layer. *Adv. Mater.* **2020**, *32*, 2002607. [CrossRef]
10. Chappert, C.; Fert, A.; Van, D.F. The Emergence of Spin Electronics in Data Storage. *Nat. Mater.* **2007**, *6*, 813–823. [CrossRef] [PubMed]
11. Prinz, G.A. Magnetoelectronics. *Science* **1998**, *282*, 1660–1663. [CrossRef]
12. Lin, H.; Gao, Y.; Wang, X.J.; Nan, T.X.; Liu, M.; Lou, J.; Yang, G.M.; Zhou, Z.Y.; Yang, X.; Wu, J.; et al. Integrated Magnetics and Multiferroics for Compact and Power-Efficient Sensing, Memory, Power, RF, and Microwave Electronics. *IEEE Trans. Magn.* **2016**, *52*, 4002208–4002215. [CrossRef]
13. Lou, J.; Liu, M.; Reed, D.; Ren, Y.H.; Sun, N.X. Giant Electric Field Tuning of Magnetism in Novel Multiferroic FeGaB/Lead Zinc Niobate–Lead Titanate (PZN-PT) Heterostructures. *Adv. Mater.* **2009**, *21*, 4711–4715. [CrossRef]
14. Hu, J.M.; Chen, L.Q.; Nan, C.W. Multiferroic Heterostructures Integrating Ferroelectric and Magnetic Materials. *Adv. Mater.* **2016**, *28*, 15–39. [CrossRef] [PubMed]
15. Ma, J.; Hu, J.M.; Li, Z.; Nan, C.W. Recent Progress in Multiferroic Magnetoelectric Composites: From Bulk to Thin Films. *Adv. Mater.* **2011**, *23*, 1062–1087. [CrossRef]
16. Yan, H.; Feng, Z.X.; Shang, S.L.; Wang, X.N.; Hu, Z.X.; Wang, J.H.; Zhu, Z.W.; Wang, H.; Chen, Z.H.; Hua, H.; et al. A Piezoelectric, Strain-controlled Antiferromagnetic Memory Insensitive to Magnetic Fields. *Nat. Nanotechnol.* **2019**, *14*, 131–136. [CrossRef] [PubMed]
17. Liu, Z.Q.; Feng, Z.X.; Yan, H.; Wang, X.N.; Zhou, X.R.; Qin, P.X.; Guo, H.X.; Yu, R.H.; Jiang, C.B. Antiferromagnetic Piezospintronics. *Adv. Electron. Mater.* **2019**, *5*, 1900176. [CrossRef]
18. Ma, C.; Luo, Z.; Huang, W.C.; Zhao, L.T.; Chen, Q.L.; Lin, Y.; Liu, X.; Chen, Z.W.; Liu, C.C.; Sun, H.Y.; et al. Sub-nanosecond Memristor Based on Ferroelectric Tunnel Junction. *Nat. Commun.* **2020**, *11*, 1439. [CrossRef]
19. Qiao, K.M.; Hu, F.X.; Liu, Y.; Li, J.; Kuang, H.; Zhang, H.R.; Liang, W.H.; Wang, J.; Sun, J.R.; Shen, B.G. Novel Reduction of Hysteresis Loss Controlled by Strain Memory Effect in FeRh/PMN-PT heterostructures. *Nano Energy* **2019**, *59*, 285–294. [CrossRef]
20. Qiao, K.M.; Wang, J.L.; Hu, F.X.; Li, J.; Zhang, C.; Liu, Y.; Yu, Z.B.; Gao, Y.H.; Su, J.; Shen, F.R.; et al. Regulation of phase transition and magnetocaloric effect by ferroelectric domains in FeRh/PMN-PT heterojunctions. *Acta Mater.* **2020**, *191*, 51–59. [CrossRef]
21. Liu, M.; Obi, O.; Lou, J.; Chen, Y.J.; Cai, Z.H.; Stoute, S.; Espanol, M.; Lew, M.; Situ, X.D.; Ziemer, K.S.; et al. Giant Electric Field Tuning of Magnetic Properties in Multiferroic Ferrite/Ferroelectric Heterostructures. *Adv. Funct. Mater.* **2009**, *19*, 1826–1831. [CrossRef]
22. Li, Q.; Tan, A.; Scholl, A.; Young, A.T.; Yang, M.; Hwang, C.; N'Diaye, A.T.; Arenholz, E.; Li, J.; Qiu, Z.Q. Electrical Switching of the Magnetic Vortex Circulation in Artificial Multiferroic Structure of Co/Cu/PMN-PT(011). *Appl. Phys. Lett.* **2017**, *110*, 262405. [CrossRef]
23. Stöhr, J.; Siegmann, H.C.; Kashuba, A.; Gamble, S.J. Magnetization Switching Without Charge or Spin Currents. *Appl. Phys. Lett.* **2009**, *94*, 072504. [CrossRef]

24. Zhang, S.; Zhao, Y.G.; Xiao, X.; Wu, Y.Z.; Rizwan, S.; Yang, L.F.; Li, P.S.; Wang, J.W.; Zhu, M.H.; Zhang, H.Y.; et al. Giant Electrical Modulation of Magnetization in $Co_{40}Fe_{40}B_{20}$/Pb($Mg_{1/3}Nb_{2/3}$)0.7$Ti_{0.3}O_3$(011) Heterostructure. *Sci. Rep.* **2014**, *4*, 3727. [CrossRef]
25. Wu, T.; Bur, A.; Wong, K.; Hockel, J.L.; Hsu, C.J.; Kim, H.K.D.; Wang, K.L.; Carman, G.P. Electric-poling-induced Magnetic Anisotropy and Electric-field-induced Magnetization Reorientation in Magnetoelectric Ni/(011) [Pb($Mg_{1/3}Nb_{2/3}$)O_3](1-x)-[$PbTiO_3$]$_x$ heterostructure. *J. Appl. Phys.* **2011**, *109*, 07D732. [CrossRef]
26. Yang, S.W.; Peng, R.C.; Jiang, T.; Liu, Y.K.; Feng, L.; Wang, J.J.; Chen, L.Q.; Li, X.G.; Nan, C.W. Non-Volatile 180° Magnetization Reversal by an Electric Field in Multiferroic Heterostructures. *Adv. Mater.* **2014**, *26*, 7091–7095. [CrossRef] [PubMed]
27. Yang, Y.J.; Yang, M.M.; Luo, Z.L.; Huang, H.L.; Wang, H.B.; Bao, J.; Hu, C.S.; Pan, G.Q.; Yao, Y.P.; Liu, Y.K.; et al. Large Anisotropic Remnant Magnetization Tunability in (011)-$La_{2/3}Sr_{1/3}MnO_3$/0.7Pb($Mg_{2/3}Nb_{1/3}$)O_3-0.3$PbTiO_3$ Multiferroic Epitaxial Heterostructures. *Appl. Phys. Lett.* **2012**, *100*, 043506. [CrossRef]
28. BinekA, C.; Chen, H.X.; Borisov, P.; Doudin, W.K. Electrically Controlled Exchange Bias for Spintronic Applications. *J. Appl. Phys.* **2005**, *97*, 10C514. [CrossRef]
29. Chen, A.T.; Zhao, Y.G.; Li, P.S.; Zhang, X.; Peng, R.C.; Huang, H.L.; Zou, L.K.; Zheng, X.L.; Zhang, S.; Miao, P.X.; et al. Angular Dependence of Exchange Bias and Magnetization Reversal Controlled by Electric-Field-Induced Competing Anisotropies. *Adv. Mater.* **2016**, *28*, 363–369. [CrossRef] [PubMed]
30. Liu, M.; Lou, J.; Li, S.D.; Sun, N.X. E-Field Control of Exchange Bias and Deterministic Magnetization Switching in AFM/FM/FE Multiferroic Heterostructures. *Adv. Funct. Mater.* **2011**, *21*, 2593–2598. [CrossRef]
31. Gong, Y.Y.; Wang, D.H.; Cao, Q.Q.; Liu, E.K.; Liu, J.; Du, Y.W. Electric Field Control of the Magnetocaloric Effect. *Adv. Mater.* **2015**, *27*, 801–805. [CrossRef]
32. Hu, Q.B.; Li, J.; Wang, C.C.; Zhou, Z.J.; Cao, Q.Q.; Zhou, T.J.; Wang, D.H.; Du, Y.W. Electric Field Tuning of Magnetocaloric Effect in $FeRh_{0.96}Pd_{0.04}$/PMN-PT Composite Near Room Temperature. *Appl. Phys. Lett.* **2017**, *110*, 222408. [CrossRef]
33. Zhao, X.Y.; Wen, J.H.; Gong, Y.Y.; Ma, S.C.; Hu, Q.B.; Wang, D.H. Nonvolatile manipulation of the magnetocaloric effect in $Ni_{43}Co_7Mn_{39}Sn_{11}$/(011)PMN-PT composite by electric fields. *Scr. Mater.* **2019**, *167*, 41–45. [CrossRef]
34. Song, C.; Cui, B.; Li, F.; Zhou, X.J.; Pan, F. Recent Progress in Voltage Control of Magnetism: Materials, Mechanisms, and Performance. *Prog. Mater. Sci.* **2017**, *87*, 33–82. [CrossRef]
35. Zhou, W.P.; Ma, C.L.; Gan, Z.X.; Zhang, Z.M.; Wang, X.X.; Tan, W.S.; Wang, D.H. Manipulation of Anisotropic Magnetoresistance and Domain Configurationin Co/PMN-PT (011) Multiferroic Heterostructures by Electric Field. *Appl. Phys. Lett.* **2017**, *111*, 052401. [CrossRef]
36. Zhao, X.Y.; Wen, J.H.; Yang, B.; Zhu, H.C.; Cao, Q.Q.; Wang, D.H.; Qian, Z.H.; Du, Y.W. Electric Field Manipulated Multilevel Magnetic States Storage in FePt/(011) PMN-PT Heterostructure. *ACS Appl. Mater. Interfaces* **2017**, *9*, 36038–36044. [CrossRef]
37. Tiercelin, N.; Dusch, Y.; Klimov, A.; Giordano, S.; Preobrazhensky, V.; Pernod, P. Room Temperature Magnetoelectric Memory Cell using Stress-mediated Magnetoelastic Switching in Nanostructured Multilayers. *Appl. Phys. Lett.* **2011**, *99*, 192507. [CrossRef]
38. Chen, Y.J.; Fitchorov, T.; Vittoria, C.; Harris, V.G. Electrically Controlled Magnetization Switching in a Multiferroic Heterostructure. *Appl. Phys. Lett.* **2010**, *97*, 052502. [CrossRef]
39. Yang, Y.T.; Wang, D.H.; Song, Y.Q.; Gao, J.L.; Lv, L.Y.; Cao, Q.Q.; Du, Y.W. Electric-field-assisted Magnetization Switching in FePd/Pb($Mg_{1/3}Nb_{2/3}$)O_3-$PbTiO_3$ Heterostructure at Room Temperature. *J. Appl. Phys.* **2013**, *114*, 144902. [CrossRef]
40. Yang, Y.T.; Zhang, Q.M.; Wang, D.H.; Song, Y.Q.; Wang, L.Y.; Lv, L.Y.; Cao, Q.Q.; Du, Y.W. Electric Field Control of Magnetic Properties in CoPt/Pb($Mg_{1/3}Nb_{2/3}$)O_3-$PbTiO_3$ Heterostructure at Room Temperature. *Appl. Phys. Lett.* **2013**, *103*, 082404. [CrossRef]
41. Peng, R.C.; Wang, J.J.; Hu, J.M.; Chen, L.Q.; Nan, C.W. Electric-field-driven Magnetization Reversal in Square-shaped Nanomagnet-based Multiferroic Heterostructure. *Appl. Phys. Lett.* **2015**, *106*, 142901. [CrossRef]
42. Peng, R.C.; Hu, J.M.; Momeni, K.; Wang, J.J.; Chen, L.Q.; Nan, C.W. Fast 180 °C Magnetization Switching in a Strain-mediated Multiferroic Heterostructure Driven by a Voltage. *Sci. Rep.* **2016**, *6*, 27561. [CrossRef] [PubMed]
43. Wang, J.J.; Hu, J.M.; Ma, J.; Zhang, J.X.; Chen, L.Q.; Nan, C.W. Full 180 °C Magnetization Reversal with Electric Fields. *Sci. Rep.* **2014**, *4*, 7507. [CrossRef]
44. Liu, M.F.; Hao, L.; Jin, T.L.; Cao, J.W.; Bai, J.M.; Wu, D.P.; Wang, Y.; Wei, F.L. Electric-field Manipulation of Coercivity in FePt/Pb($Mg_{1/3}Nb_{2/3}$)O_3–$PbTiO_3$ Heterostructures Investigated by Anomalous Hall Effect Measurement. *Appl. Phys. Express* **2015**, *8*, 063006. [CrossRef]
45. Li, P.S.; Chen, A.T.; Li, D.L.; Zhao, Y.G.; Zhang, S.; Yang, L.F.; Liu, Y.; Zhu, M.H.; Zhang, H.Y.; Han, X.F. Electric Field Manipulation of Magnetization Rotation and Tunneling Magnetoresistance of Magnetic Tunnel Junctions at Room Temperature. *Adv. Mater.* **2014**, *26*, 4320–4325. [CrossRef]
46. Wu, T.; Zhao, P.; Bao, M.Q.; Bur, A.; Hockel, L.J.; Wong, K.; Mohanchandra, K.P.; Lynch, C.S.; Carman, G.P. Domain Engineered Switchable Strain States in Ferroelectric (011)[Pb($Mg_{1/3}Nb_{2/3}$)O_3]$_{(1-x)}$-[$PbTiO_3$]$_x$ (PMN-PT, x = 0.32) Single Crystals. *J. Appl. Phys.* **2011**, *109*, 124101.